Robust and leaky transport barriers in unstable baroclinic flows

J. G. Esler[a)]
Department of Mathematics, University College London, 25 Gower Street, London WC1E 6BT, United Kingdom

(Received 29 April 2008; accepted 15 October 2008; published online 17 November 2008)

Unstable baroclinic jets undergoing life cycles of wave growth and nonlinear equilibration are investigated numerically in a quasigeostrophic two-layer model. The focus is on understanding the properties of the upper layer transport barrier that emerges in the ensuing turbulent flow. The transport barriers in the simulated flows are representative of observed atmospheric and oceanic transport barriers, for example, at the extratropical tropopause, or at the Atlantic Gulf stream or the Antarctic circumpolar current. The simulations reveal that, depending on the value of the (inverse) criticality parameter β associated with the initial jet, the developing transport barriers either remain almost entirely impermeable to transport or "leak" by allowing vortices to be shed across them. A dynamical theory to predict the final flow, based on minimization of potential energy subject to relevant kinematic and dynamical constraints, is extended to make predictions about the transport barrier behavior. The theory is able to predict the value of β for which the barrier begins to leak and provides accurate estimates for the ensuing potential vorticity exchange across the barrier, which is primarily due to the vortex shedding. © *2008 American Institute of Physics*.
[DOI: 10.1063/1.3013631]

I. INTRODUCTION

It is well established that geostrophic turbulence, in the presence of a sufficiently strong gradient of planetary vorticity leads to the formation of jets.[1,2] In the Earth's atmosphere and oceans[3–5] and on the giant planets,[6–9] eastward (or cyclonic) jets tend to be narrower and more energetic than their westward counterparts. A dynamical explanation, based primarily on the results of numerical simulations, but generally supported by observations, is reviewed in detail in the recent perspective of Dritschel and McIntyre.[10] They proposed that jet formation occurs by a process of (horizontal) layerwise potential vorticity (PV hereafter) mixing. Due to the invertibility property of PV, the resulting layered pattern almost entirely determines the flow, and the resulting flow exhibits the observed asymmetry between eastward and westward jets. The eastward jets are colocated with the interfaces between the layers and can be identified with sharp gradients or jumps in PV, whereas the broader westward jets are associated with the homogeneous layers themselves.

One important consequence of the jet formation process described above is that the eastward jets/PV jumps act as transport barriers. The stirring and mixing of tracers in directions parallel to such barriers can be many times greater than that across them.[11] The barrier effect is often attributed to "Rossby wave elasticity,"[12] so-called because in regions where PV gradients are strong, i.e., at a PV jump, Rossby wavelike motions will persist, whereas where they are weak PV gradients can easily be overcome, initiating turbulence and mixing. Various techniques, including the calculation of contour lengthening rates,[13] and "effective diffusivity"[14] (a measure of diffusion across tracer isopleths in a tracer-following coordinate system) have been used to identify and analyze such transport barriers in the atmosphere and oceans. These techniques clearly reveal examples of transport barriers at the extratropical tropopause in each hemisphere,[15] at the edge of the stratospheric winter polar vortex,[16] at the Antarctic circumpolar current,[5] and at the Atlantic Gulf stream.[17,18] The persistence of the observed transport barriers in many cases is supported by measurements revealing strong chemical tracer gradients across the jet region.

The focus here will be on those transport barriers where geostrophic turbulence is initiated by the baroclinic instability of a single isolated jet, as occurs at the extratropical tropopause and at various ocean currents.[19] There is considerable variability in the observed behavior of such transport barriers in nature. In the winter hemisphere, trajectory studies using large-scale winds[20] reveal that very few, if any, trajectories cross the tropopause barrier within a layer bounded in the vertical by the 330–370 K isentropic surfaces. The winter extratropical tropopause barrier might therefore be described as robust to transport within this layer. In contrast, it is well known[21] that in the summer considerably more transport takes place across the tropopause in both hemispheres. Hence, the summer tropopause barrier might be described as "leaky." Greenslade and Haynes[22] recently demonstrated in three-dimensional numerical simulations that the "leakiness" of a horizontal transport barrier can also vary significantly in the vertical; and significant vertical structure also appears to exist at the tropopause.[20] Another, more distinctive example of a leaky transport barrier flow is the North Atlantic Gulf-stream current.[17,18] At surface levels a strong gradient in water mass properties exists across the current, indicating a transport barrier. Nevertheless, both cyclonic and anticyclonic vortices ("warm-core rings" and "cold-core rings") are repeatedly shed across the main current. Conse-

a)Electronic mail: gavin@math.ucl.ac.uk.

quently, there is intermittent exchange between the water masses on either side of the main current. What controls the rate of exchange between them?

The persistence of transport barriers and the transition between "robust" and "leaky" barriers have been widely studied in a kinematic context. Typically, ideas from dynamical systems theory are used to investigate the behavior of a prescribed time-periodic flow when an amplitude parameter is varied.[23] In such studies the most resilient barrier to transport is typically found to be colocated with a jet axis. At low values of the amplitude parameter, this barrier is robust, and as the amplitude parameter is increased it begins to leak and eventually is completely destroyed. One criticism of this line of study, concerning its relevance to geophysical flows, is that the prescribed flow is not "dynamically consistent" in the sense that it is not determined by a PV distribution that is conserved following the flow. Recently, in a series of numerical experiments, Haynes *et al.*[24] compared the barrier behavior in two closely analogous flows, one kinematically prescribed and the other dynamically consistent. Interestingly, they found that dynamical consistency increases the tendency for the transport barrier to either be robust or to completely and abruptly break down, leading to a greatly reduced region of parameter space in which the barrier is leaky.

The current work aims to bring an alternative, dynamical perspective to the question of why some atmospheric and oceanic transport barriers leak and others do not. Idealized, unforced, initially unstable baroclinic "life cycle" flows are investigated in a quasigeostrophic two-layer model as a paradigm for the unstable baroclinic flows that lead to transport barrier formation in the atmosphere and ocean. A recent theory, introduced by the author[25] (E08 hereafter), for the turbulent equilibration of such unstable baroclinic flows is re-examined and extended to make predictions about the permeability of the developing transport barrier associated with the upper layer jet (see, e.g., Fig. 1 of Greenslade and Haynes[22] for a schematic illustrating how the upper layer transport barrier can be considered to be a model "tropopause"). The theory is based on the idea that the flow seeks to minimize the available potential energy (APE hereafter) under certain constraints and allows predictions based on knowledge of the initial flow only. The theory is formulated at present only for unforced, initially unstable flows, but the intention is that the resulting predictions will provide insight into the behavior of the more realistic forced-dissipative flows observed in nature, such as those described above.

Section II introduces the idealized baroclinic flows under investigation and the setup of the numerical model experiments. In Sec. III the theoretical framework of E08 is reintroduced together with a general formalism that allows extension of the theory into the leaky barrier regime. In Sec. IV the predictions of the theory and the results of the numerical simulations are compared, and in Sec. V conclusions are given.

II. MODEL EQUATIONS AND BACKGROUND

A. Physical scenario and model equations

The quasigeostrophic two-layer model[26] describes flow in a recirculating channel that is periodic in the x-direction (longitude), with length L_x, and has sidewalls at fixed latitudes $y=\pm L_y/2$. The channel, which represents a latitude band in the extratropics of a rotating planet, rotates at rate $f/2$, where under the β-plane approximation[27] it is taken that $f=f_0+\beta^* y$. The upper and lower fluid layers, each have undisturbed depth H, evolve under gravity g and have densities ρ_1 and $\rho_2(>\rho_1)$, respectively. It is taken that $2(\rho_2-\rho_1)/(\rho_1+\rho_2)\ll 1$, in order that the Boussinesq approximation may be used, i.e., a "reduced gravity" $g'=2g(\rho_2-\rho_1)/(\rho_1+\rho_2)$ acts on the interface between the layers and the pressure field at the upper layer free surface is identical to that in the presence of a rigid lid. The evolution of an initially unstable upper layer jet, flowing in the positive x-direction (eastward) with maximum velocity U is to be considered. The flow is viscous with kinematic viscosity ν^*. Interfacial and bottom frictions are neglected. Following previous studies,[27,28] the equations of motion for a rotating two-layer shallow fluid can be nondimensionalized, taking horizontal length scales equal to the internal Rossby radius $L_D=\sqrt{g'H/2f_0^2}$, vertical length scale H, time scale L_D/U, and horizontal and vertical velocity scales U, UH/L_D. Under the quasigeostrophic approximation, the resulting equations of motion are[27]

$$\frac{D_i q_i}{Dt}=\kappa\nabla^4\psi_i, \quad i=1,2, \tag{1}$$

$$q_i\equiv\beta y+\nabla^2\psi_i+(-1)^i\left(\frac{\psi_1-\psi_2}{2}\right), \tag{2}$$

$$\frac{D_i}{Dt}\equiv\partial_t-\psi_{iy}\partial_x+\psi_{ix}\partial_y. \tag{3}$$

Here, ψ_i is the geostrophic stream function in each layer $(i=1,2)$, which determines the geostrophic velocity via $(u_i,v_i)=-\nabla\times\psi_i\mathbf{k}$, and q_i is the quasigeostrophic potential vorticity. The stream function ψ_i is subject to boundary conditions

$$\psi_{ix}=0, \quad \bar{\psi}_{iy}=-U_i^{\pm} \quad \text{on} \quad y=\pm\frac{L_y}{2}, \quad i=1,2, \tag{4}$$

where the overbar denotes an x-average (zonal average), and $U_i^{\pm}$ are the initial velocities at the sidewalls in each layer.

The nondimensional parameters in Eqs. (1)–(3) are

$$\beta=\frac{\beta^* L_D^2}{U}, \quad \kappa=\frac{\nu^*}{UL_D}.$$

The inverse criticality β is a measure of the degree of instability of the jet, while κ is an inverse (Rossby–)Reynolds number and measures the importance of viscous effects. The initial jet is chosen to have latitudinal profile,[29]

$$U_1 = -\psi_{1y} = \mathrm{sech}^2\left(\frac{y}{\sigma}\right), \quad U_2 = -\psi_{2y} = 0. \tag{5}$$

The parameter σ is the jet half-width in nondimensional units (i.e., $\sigma = W/L_D$ for physical jet half-width W). Note that the lower layer sidewall velocities $U_2^{\pm} = 0$, and for the values of σ used below, the upper layer sidewall velocities $U_1^{\pm} \approx 0$. To retain the focus on single-jet baroclinic instability, several restrictions on the value of σ are necessary, as discussed in detail in E08. In summary, for σ too low ($\lesssim 1.5$) the instability of the jet changes character to mixed barotropic-baroclinic type, whereas for σ too high ($\gtrsim 6$) multiple jet formation is possible.[29]

In the current study, jet widths of $\sigma = 2$ and $\sigma = 3$ are chosen for the simulations in order to minimize the influence of the sidewalls on the flow evolution. With atmospheric parameters these values result in latitudinal flow profiles with (physical) jet half-widths $W \approx 1600-2400$ km, comparable to the extratropical tropospheric jets. In the case of oceanic jets, the corresponding half-widths are in the range $W \approx 100-150$ km. For the criticality parameter β, despite the fact that the qualitative behavior of typical two-layer model flows closely resembles those observed in the atmosphere and ocean, there are well-known pitfalls[30] associated with making exact quantitative comparisons between two-layer flows and observed oceanic and atmospheric flows. Note also that, as a first step, the current study focuses on unforced life cycles rather than the forced-dissipative flows typically observed in nature. Consequently, it is difficult to determine a single definitive value of β that exactly corresponds to an observed flow. However, as discussed in E08, the behavior of the extratropical tropospheric jets in the atmosphere clearly resembles that of two-layer flows with $0.15 \lesssim \beta \lesssim 0.3$, while much lower values of β ($\lesssim 0.05$) are relevant for the most energetic oceanic currents, such as the Gulf Stream. For the Rossby–Reynolds number κ, in both atmosphere and ocean, the relevant value of κ (approximately 5×10^{-13} and 2×10^{-10}, respectively, if molecular kinematic viscosities are used) is much lower than can be attained in the numerical simulations. However, in E08 it was demonstrated that for $\kappa \lesssim 1 \times 10^{-3}$ zonal mean fields at the end of the life cycle are essentially independent of κ. The channel length and width are set to $L_x = 20\pi$ and $L_y = 7\pi$ (Rossby radii L_D), respectively. These values are approximately appropriate if the channel corresponds to the extratropical troposphere. Note that the channel width has been increased relative to that in E08 in order to minimize sidewall effects.

To initialize the numerical simulations described below, a perturbation with the form

$$\tilde{q}_1(x,y) = \varepsilon\left(x - \frac{L_x}{2}\right) e^{-((x - L_x/2)^2 + y^2)/R^2}$$

is added to the initial upper layer PV field. In all simulations described below $\varepsilon = 0.04$ and $R = 2$. Note that the initial perturbation $\tilde{q}_1$ is localized in physical space (as opposed to being a periodic wave) in order that the fastest growing disturbances may naturally emerge during the subsequent evolution. This approach avoids biasing the results by removing any artificial symmetry associated with a particular zonal wavenumber.

B. Numerical implementation and experiments

The numerical model[31] used to obtain solutions of Eqs. (1)–(4) exploits a standard pseudospectral representation in the x-direction and a grid point representation in the y-direction. At fixed numerical resolution, converged solutions of Eq. (1) can be obtained only for values of κ greater than some threshold value. Diffusivity greater than the threshold value is necessary to prevent the forward cascade of enstrophy in wavenumber space from causing a spurious buildup of enstrophy at the model grid scale, i.e., the effective Kolmogorov microscale (here $\kappa^{1/2} L_D$) must be resolved by the model grid.

For the set of experiments reported below, 1024 Fourier modes are used in the x-direction and 641 grid points in the y-direction. The time step is set to 5×10^{-4} nondimensional time units (scaled on f_0^{-1}). In practice, the value of the diffusivity parameter, set close to the lowest value necessary to maintain numerical stability and obtain converged solutions, is $\kappa = 4 \times 10^{-4}$. The equations are integrated for a time $T = 300 f_0^{-1}$, by which time, as discussed further below, the baroclinic life cycle is essentially complete.

For fixed channel dimensions, and sufficiently low κ, the outcome of the simulations depends on only two parameters, namely, the inverse criticality and nondimensional jet width (β, σ). The transport barrier behavior is found to be considerably more sensitive to β, hence the particular focus here is on determining the detailed behavior in the range $\beta \in [0.12, 0.3]$, with two different jet widths $\sigma = 2$ and 3 used to validate the theory further. The limited range of β is sufficient to capture the transition between a robust and leaky upper layer transport barrier. For each jet width, then, experiments are conducted at intervals in β of 0.02. Note that for $\beta \lesssim 0.1$ the channel width necessary to prevent sidewall effects becoming important increases rapidly with decreasing β. Hence, this region of parameter space is not investigated here.

III. LIFE CYCLE BEHAVIOR AND THEORETICAL FORMULATION

A. Baroclinic life cycle behavior

The qualitative behavior during two-layer baroclinic life cycles is described in detail in E08. A brief summary follows. The perturbed jet undergoes a period of linear wave growth, and the most unstable linear mode of the flow emerges. The growing waves eventually saturate in amplitude and break in both layers: to the flanks of the jet in the upper layer and across the center of the channel in the lower layer. As discussed by, e.g., Nakamura[32] and Yuan *et al.*,[19] in the atmospheric and oceanic contexts, respectively, aspects of the subsequent nonlinear behavior can be deduced from the structure of the most unstable linear mode. In particular, the subsequent locations of the upper layer mixing zones are approximately coincident with the critical lines of the linear mode. During the final stage of the life cycle, turbulence

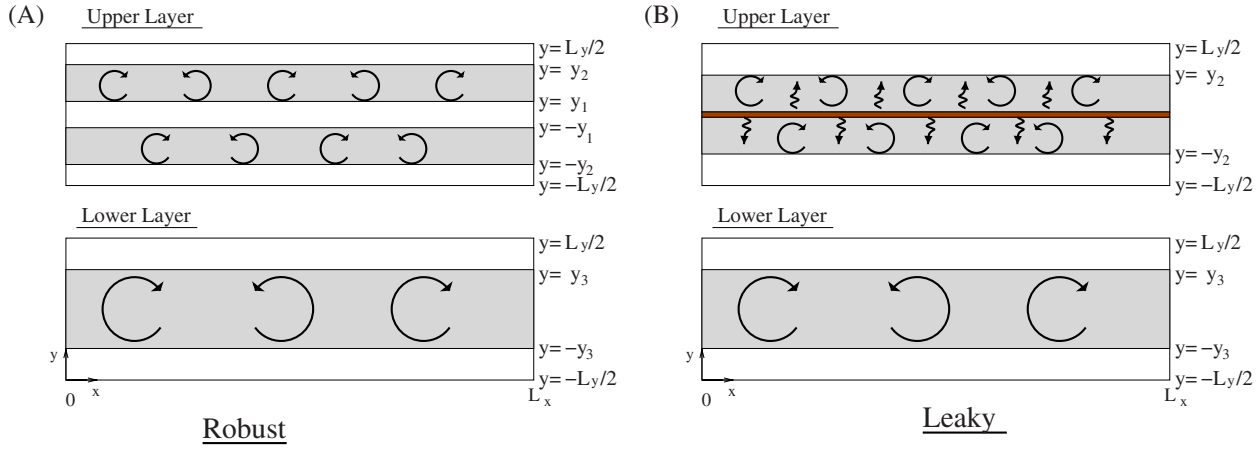

FIG. 1. (Color online) Schematic illustrating nature of potential vorticity mixing in flows with (a) a robust and (b) a leaky upper layer transport barrier.

ensues in the wave breaking regions in the upper and lower layers, leading to PV homogenization within those regions.

Examination of the energy budget, as in E08, reveals that, for sufficiently small κ as here, the total energy is conserved to a good approximation during the life cycles. Available zonal mean potential energy is converted to eddy energy during the early stages of the life cycle, and in the latter stages the eddy energy is returned to the zonal mean, mainly as kinetic energy. This latter process, known as "barotropic decay,"[32] is consistent with an almost entirely nondissipative decay of the deformation-scale eddies and eventually results in the acceleration of the jet in both layers. In the simulations reported here, the energetic cycle described above is essentially complete by the time $T=300f_0^{-1}$, taken as the end of the life cycles.

B. Representation of eddy-induced changes to the initial potential vorticity distribution

In the limit of low diffusivity κ, the action of eddies on the initial PV distribution, in the first instance, is to rearrange that distribution conservatively. The effect of a conservative redistribution of the initial PV field is such that the new PV distribution can be obtained from the initial distribution by a parcelwise rearrangement, followed by the action of a smoothing or coarse-graining operation consistent with the presence of weak diffusion.

Here, we aim to generalize the approach to PV mixing taken in E08, the concept behind which is illustrated schematically in Fig. 1(a). In E08 it was assumed that eddies act to homogenize PV within well-delineated regions, located to the flanks of the jet in the upper layer (specifically the regions $y\in[-y_2,-y_1]$ and $y\in[y_1,y_2]$) and across the center of the channel in the lower layer ($y\in[-y_3,y_3]$), as shown. In conjunction with the minimization principle of E08 (reviewed below), this PV mixing assumption led to accurate predictions of the final flows in the E08 simulations over a range of criticalities (approximately $\beta\in[0.225,0.325]$). The predictions of E08 were less accurate, however, at higher criticalities ($\beta\approx0.2$) where the inner boundary of the upper layer mixing regions, given by latitude y_1, approaches the center of the channel ($y_1\to0$). In simulations with $\beta\lesssim0.2$, the central barrier to mixing retains a finite width despite the prediction $y_1\to0$ and, unlike flows at lower criticality (higher β), PV mixing across the central barrier is observed.

To extend the theory of E08 in line with the results of the simulations, a mixing operator is required that will either homogenize PV in distinct regions to the jet flanks, as illustrated schematically in Fig. 1(a), or allow additional mixing across a central barrier in addition to the homogenization, as illustrated in Fig. 1(b). The former mixing regime will be referred to as the "robust barrier regime" and the latter the "leaky barrier regime." By allowing for these two possible regimes, the minimization principle of E08 can be applied, and the theory of E08 extended, to make predictions about the transition between them. It is to be emphasized that no *a priori* assumptions about which regime is appropriate for a particular initial flow will be made; this aspect will be entirely determined by the extended theory.

To proceed, a mixing operator $\mathcal{L}_i$ is defined that allows the final PV profiles $q_i(y)$ in each layer ($i=1,2$) to be expressed in terms of the corresponding initial profiles $Q_i(y)$. It is convenient to choose a linear Fredholm integral operator of the form

$$q_i=\mathcal{L}_i[\mathbf{y},\delta]\cdot Q_i\equiv\int_{-L_y/2}^{L_y/2}K_i(y,y'|\mathbf{y},\delta)Q_i(y')dy'. \tag{6}$$

The idea is that the integral kernels K_i can be chosen to depend smoothly on both a vector of latitudes $\mathbf{y}^T=\{y_1,y_2,y_3\}$ that specify the locations of the boundaries of the mixing regions as shown in Fig. 1, and a "smoothness parameter" δ that determines the sharpness of the edges of those mixing regions. Several constraints on K_i are necessary if the operator $\mathcal{L}_i$ is to represent the effect of eddies on the initial flow. In order for eddy mixing to conserve the total PV in each layer, it is necessary that

$$\int_{-L_y/2}^{L_y/2}K_i(y,y'|\mathbf{y},\delta)dy=1\quad\text{for all}\quad y'\in\left[-\frac{L_y}{2},\frac{L_y}{2}\right], \tag{7}$$

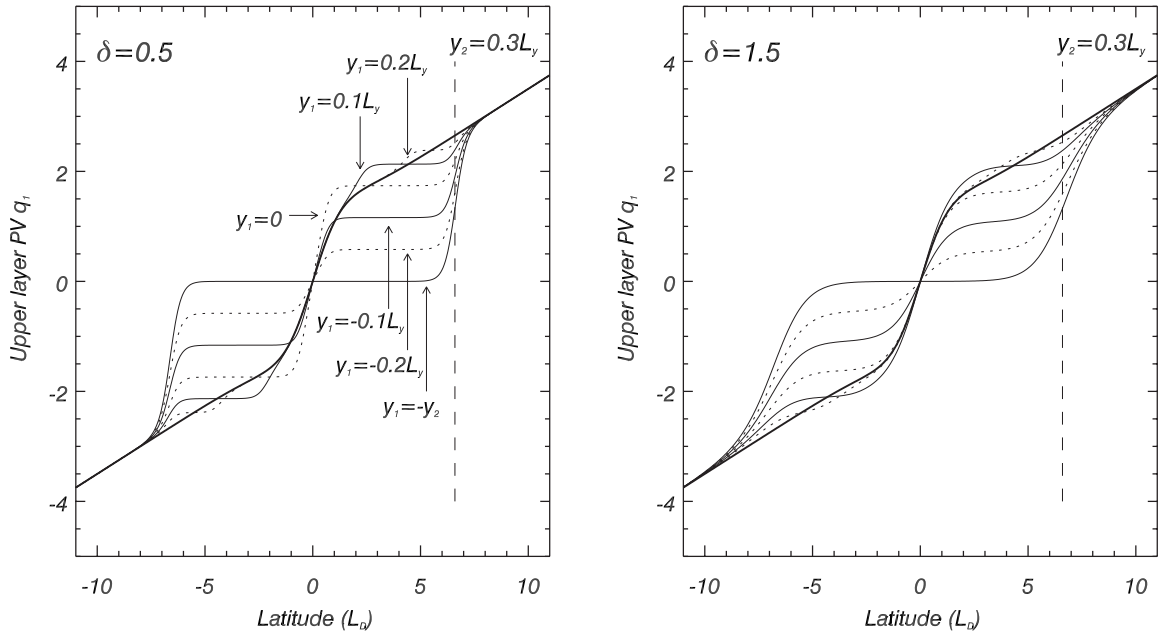

FIG. 2. Illustrating the action of various configurations of the mixing operator $\mathcal{L}_1[\mathbf{y},\delta]\cdot$, defined by Eqs. (A2) and (A3), on the PV profile $Q_1(y)$ (solid, bold) for the initial flow with $\beta=0.25$, $\sigma=2$, and $L_y=7\pi$. Left: $y_2=0.3L_y$, $y_1=-y_2,-0.2L_y,-0.1L_y,0,0.1L_y,0.2L_y$, $\delta=0.5$. Right: Same as in the left panel but with the smoothness parameter $\delta=1.5$.

$$\int_{-L_y/2}^{L_y/2} K_i(y,y'|\mathbf{y},\delta)dy' = 1 \quad \text{for all} \quad y \in \left[-\frac{L_y}{2},\frac{L_y}{2}\right]. \tag{8}$$

Condition (7) ensures that PV is conserved under the action of $\mathcal{L}_i$. Condition (8) arises because the flow is incompressible, i.e., each fluid particle in the final flow must be a combination of fluid particles from the initial flow with an equivalent total volume. A further condition, to ensure that eddy mixing of PV will, in general, act to rearrange the initial PV field conservatively and that, in particular, there is no generation of new PV values outside the range $[\text{Min}\{Q_i(y)\},\text{Max}\{Q_i(y)\}]$, is that

$$K_i(y,y'|\mathbf{y},\delta) \geq 0, \quad \text{for all} \quad y,y' \in \left[-\frac{L_y}{2},\frac{L_y}{2}\right]. \tag{9}$$

Operators satisfying Eqs. (7)–(9) acting on two-dimensional vorticity fields have been described as "polymorphisms," see, e.g., Arnold and Khesin (Ref. 33, p. 82) and Shnirelman.[34] Polymorphisms span all the possible states that are permissible due to mixing the initial vorticity field. These include all of the possibilities between the extreme states represented on the one hand by parcelwise rearrangement of fluid particles ("area-preserving diffeomorphisms") and on the other by complete homogenization of the vorticity field.

To proceed, an explicit form is needed for the kernel K_i in each layer. The full details of the explicit expressions chosen, in order to satisfy the above properties and to generate the desired mixing behavior, are outlined in the Appendix. However, to give an impression of the action of the resulting operator $\mathcal{L}_1$ on the initial upper layer PV profile $Q_1(y)$ for a typical flow (with $\beta=0.25$, $\sigma=2$, $L_y=7\pi$), Fig. 2 shows the mixed profiles $q_1(y)$ that result when the operator is applied at several different variable settings. The left panel shows results for smoothness parameter $\delta=0.5$ and the right panel $\delta=1.5$, and the outer boundary of the mixing region is fixed in each case at $y_2=0.3L_y$. The bold curve is the initial profile $Q_1(y)$, and the remaining curves show the mixed profile results for values of the "inner" latitude variable $y_1=0.2L_y$, $0.1L_y$, 0, $-0.1L_y$, $-0.2L_y$, and $-0.3L_y$ $(=-y_2)$. For $y_1>\delta$, the mixing operator is in the robust barrier regime and y_1 may be interpreted as determining the latitudes of the inner boundaries of the upper layer mixing region, as in Fig. 1(a). For $y_1\leq\delta$, the mixing operator is in the leaky barrier regime and in this regime y_1 instead controls the extent of mixing across the barrier, as suggested in Fig. 1(b). When $y_1=-y_2$, the minimum possible value for y_1, the central mixing barrier, disappears completely and a single mixing region spans $[-y_2,y_2]$.

The assumption that the eddies act according to Eq. (6), with the specific Fredholm integral operator chosen here, can be regarded as a reduction in the dimensionality of the problem of finding the end state of the life cycles. In effect, the observed self-similarity of the action of the eddies on the initial PV profile, together with an assumption of symmetry about the channel center, is being exploited to reduce the entire problem to one of determining the three unknown latitude variables $\{y_1,y_2,y_3\}$.

The reduction to three latitude variables, as opposed to any other number, is essentially arbitrary except that it is sufficient to describe, although crudely, the qualitative PV mixing behavior observed across all of the simulated life cycles. Further mixing regions and /or more latitude variables might easily be introduced, for example, by breaking the assumption of symmetry about the channel center, but at

the expense of increasing the dimensionality of the problem. Experimentation with different versions of the operator kernels K_i has revealed that their exact form is not critically important in determining the results described below. Given an alternative mixing operator, provided that the qualitative effect on the initial PV profile remains that of PV homogenization within well-delineated regions, very similar results to those presented can be found for the alternative formulation (e.g., a tanh profile has been assumed for the upper layer leaky regime PV profile in $[-y_2, y_2]$ with similar results to those reported below). The final aspect of the mixing operator that must be discussed regards the smoothness parameter δ. It is assumed here that the value of δ is determined by the detailed dynamics occurring on the PV interface associated with the barrier itself, including dissipative processes occurring there, rather than by the large-scale flow, and that δ will be of the order of the Rossby radius (i.e., $\delta \approx 1$). Results for several values of δ will be given in order to establish that it does not play a major qualitative role in the theory established below.

C. Equilibration via potential vorticity homogenization theory and its extension to the leaky barrier regime

In E08 a theory was presented, equilibration via potential vorticity homogenization (EPVH), which predicts the final state of baroclinic life cycles as a function of the initial flow parameters (β, σ). An assumption that a robust transport barrier exists in the upper layer of the flow, throughout the life cycle, is implicit in E08. Here, the generalization of the mixing operator described above will allow an extension of the EPVH ideas into the leaky barrier regime.

Specifically, the EPVH theory of E08 aims to predict the locations of the boundaries of the mixing regions, as described by the latitude variables $\mathbf{y}^T = \{y_1, y_2, y_3\}$, as a function of the flow parameters (β, σ). The prediction derives from minimizing the potential energy

$$V = \frac{1}{4}\int (\psi_1 - \psi_2)^2 d^2\mathbf{x}, \tag{10}$$

subject to constraints on the conserved quantities of energy

$$E = \frac{1}{2}\int |\nabla\psi_1|^2 + |\nabla\psi_2|^2 + \frac{(\psi_1 - \psi_2)^2}{2} d^2\mathbf{x} \tag{11}$$

and zonal momentum

$$M = \int u_1 + u_2 d^2\mathbf{x}. \tag{12}$$

Energy and momentum are taken to be equal to their initial values at the end of the simulations, i.e., $E = E_0$, $M = M_0$ as would be the case were the flow entirely inviscid. It is further assumed that by the end of the life cycles the energy E and potential energy V are well approximated by their zonal means, denoted as $\bar{V}$ and $\bar{E}$. These latter assumptions are justified by the nondissipative decay of the eddy field observed toward the end of the life cycles in the simulations. For fixed flow parameters (β, σ), a nonlinear system is defined and solved to find $\mathbf{Y}^T = \{Y_1, Y_2, Y_3\}$, i.e., those values of the latitude parameters $\mathbf{y}$ that minimize $\bar{V}$ subject to $\bar{E} = E_0$ and $M = M_0$.

The E08 predictions for the final flow field are then easily obtained from $\mathbf{Y}$. In terms of the mixing operator defined by Eq. (6) above, the E08 prediction for the final PV field $q_i(y)$ in terms of the initial field $Q_i(y)$ is given by

$$q_i(y) = \mathcal{L}_i[\mathbf{Y}, 0] \cdot Q_i(y).$$

The profiles q_i fully define the final state of the life cycle, as the final stream function ψ_i can be obtained by inversion, i.e., solving the elliptic equation defined by Eq. (2) together with the boundary conditions. The zonal mean flow profiles $u_i = -\psi_{iy}$ and interface height $[= (\psi_2 - \psi_1)/2]$ follow. E08 analyzed the success of predictions based on the above theory compared with the calculated "final" flows in simulated life cycles. The predictions were found to be accurate over a large but bounded region of (β, σ) parameter space. E08 also found that the reasons for the breakdown of the theory outside the region of validity were clear from the theory itself. In particular, it was found that $Y_1 \to 0$ as β decreased, hinting at the onset of the leaky barrier regime.

The main aim behind introducing the mixing operator formalism above is to enable a straightforward extension of the E08 theory to a wider region of (β, σ) parameter space, in order to make predictions for those flows in the leaky barrier regime. In general, a standard technique to find the latitude variables $\mathbf{Y}$ that minimize potential energy, subject to the constraints on energy and momentum, is to proceed by finding the critical points of the function

$$F(\mathbf{y}|\delta) = \bar{V}(\mathbf{y}|\delta) + \lambda\bar{E}(\mathbf{y}|\delta) + \mu M(\mathbf{y}|\delta), \tag{13}$$

where λ and μ are Lagrange multipliers. Provided that the critical point found corresponds to a minimum of F, the unknowns $\{\mathbf{Y}, \lambda, \mu\}$ are determined by the solution of the corresponding system of equations

$$\frac{\partial F}{\partial \mathbf{y}}(\mathbf{Y}|\delta) = 0, \quad \bar{E}(\mathbf{Y}|\delta) = E_0, \quad M(\mathbf{Y}|\delta) = M_0. \tag{14}$$

Roots of Eq. (14) can be found numerically, using a multidimensional nonlinear root finder (e.g., Broyden's method[35]). To implement a root finding algorithm it is necessary to have explicit expressions for the partial derivatives of F with respect to $\mathbf{y}$. After some working, these can be expressed in terms of the partial derivatives of the mixing kernels as

$$\frac{\partial F}{\partial \mathbf{y}}(\mathbf{y}|\delta) = \sum_{i=1}^{2}\int_{-L_y/2}^{L_y/2}\int_{-L_y/2}^{L_y/2}\left(\frac{(-1)^{i+1}}{2}\phi(y) - \lambda\psi_i(y) + \mu y\right) \times \frac{\partial K_i}{\partial \mathbf{y}}(y, y'|\mathbf{y}, \delta)Q_i(y')dydy', \tag{15}$$

where ϕ is defined by

$$\phi_{yy} - \phi = (\psi_1 - \psi_2), \quad \phi_y = 0 \quad \text{on} \quad y = \pm\frac{L_y}{2}.$$

The partial derivatives of K_i with respect to $\mathbf{y}$ are straightforward to evaluate for the particular examples used here (see

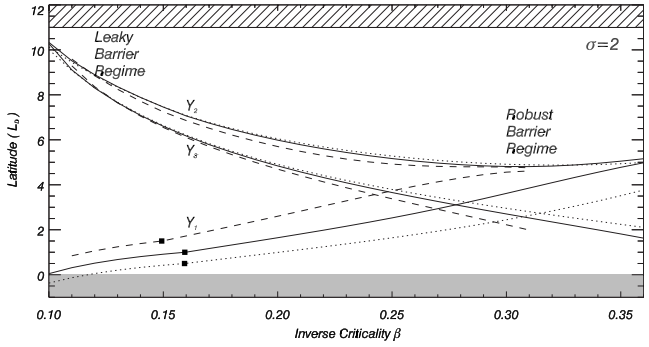

FIG. 3. The solutions $\{Y_1, Y_2, Y_3\}$ of the nonlinear Eq. (14), illustrating the boundaries of the mixing regions, for the case with jet width $\sigma=2$, as a function of inverse criticality β for $\beta \in [0.1, 0.36]$, for different values of the smoothness parameter δ ($\delta=0.5$ dotted, $\delta=1$ solid, and $\delta=1.5$ dashed). Solid points show the position of the change in character of the mixing operator $Y_1=\delta$ from the leaky to robust regimes [see Eqs. (A2) and (A3)].

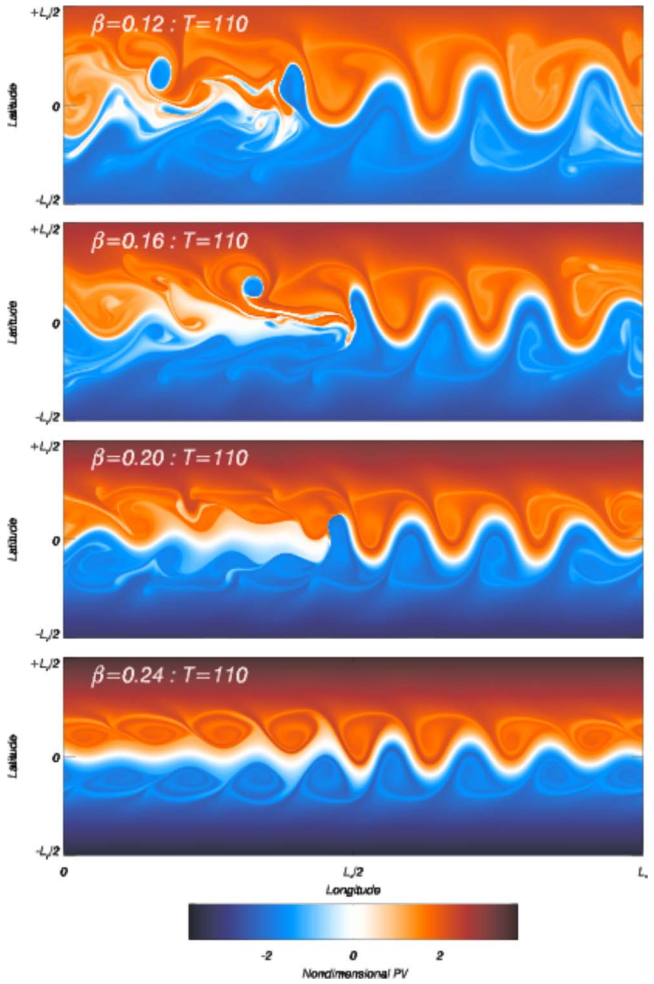

FIG. 4. (Color online) Snapshots of upper layer PV at $t=110f_0^{-1}$ for the $\sigma=2$ jet case. Simulations with $\beta=0.12$, 0.16, 0.20, and 0.24 are shown.

the Appendix). Note that Eqs. (3.4) and (3.5) in E08 are simply a special case of Eq. (15) for the specific kernels used in that work.

For fixed flow parameters (β, σ), a single, apparently unique, solution for $\mathbf{Y}$ is typically found from Eq. (14). It is straightforward to verify that such a solution is a local minimum of F (see E08). For a fixed jet width $\sigma=2$, Fig. 3 shows the solutions $\mathbf{Y}^T=\{Y_1, Y_2, Y_3\}$ as a function of β for three different values of the smoothness parameter ($\delta=0.5$ dotted, $\delta=1$ solid, and $\delta=1.5$ dashed). At high β, the theory predicts that the PV mixing regions $[-Y_2, -Y_1]$, $[Y_1, Y_2]$ (upper layer) and $[-Y_3, Y_3]$ (lower layer) are relatively narrow. As β decreases, the mixing regions are predicted to increase in size, until as $\beta \lesssim 0.2$, $Y_1 \to 0$ and Y_2 and Y_3 begin to approach the channel walls, so that the mixing regions span nearly the entire channel. Of the three latitude variables, only Y_1 is found to be sensitive to the smoothness parameter δ. Nevertheless, the value of $\beta \approx 0.16$ where the mixing kernel changes character from robust to leaky type is relatively independent of δ. For low values of β (≈ 0.1), Y_1 is significantly less than δ in each case, indicating that significant cross-jet mixing is predicted. This prediction will be evaluated below.

IV. RESULTS

A. Robust and leaky transport barriers in the simulations

The baroclinic life cycles in the simulation undergo a sequence of linear wave growth, nonlinear saturation and wave breaking, and finally layerwise turbulence and wave decay. The latter stage is often referred to as barotropic decay in the atmospheric dynamics literature[36] and, importantly, it is a nondissipative process. As shown explicitly in E08, the total energy E is conserved to a good approximation throughout the life cycles. By the end of the life cycles, at a time taken here to be $T=300f_0^{-1}$, the turbulence is relatively weak and the mean flow is close to steady in time, the influence of dissipation on the large-scale mean flow being negligible on the time scale of the life cycles. It is this near-steady end state that we seek to predict using the extended EPVH theory described above.

The question of how the simulated life cycles differ qualitatively as a function of β can be addressed by examining snapshots of upper layer PV q_1. Figure 4 shows q_1 at a fixed time ($t=110f_0^{-1}$) during four different simulations with $\beta=0.12$, 0.16, 0.20, and 0.24, and $\sigma=2$. The snapshots show the wave development during the nonlinear saturation/wave breaking stage of the life cycles. The upper layer transport barrier is visible in each panel as a thin white band separating the northern ($y>0$) and southern ($y<0$) sections of the channel. In each simulation, sharp PV gradients in the barrier region support finite amplitude baroclinic Rossby waves, which have developed from the initial instability and are eastward propagating. The amplitude of the waves differs somewhat between the simulations, with the largest waves occurring for the lowest values of β. The striking difference between the four simulations, however, is in the manner in which the waves are seen to break. At low β large vortices are shed across the transport barrier. Later snapshots (not shown) reveal that this vortex shedding is bidirectional and is a continuous process occurring throughout the most active stage of the life cycle (approximately $t=80f_0^{-1}-220f_0^{-1}$), and

occurs at all longitudes in the channel. For the $\beta=0.16$ simulation, the vortex shedding is still present, but the vortices are much smaller. At $\beta=0.20$, no significant vortex shedding occurs, but very sharp PV gradients at the trailing edge of the developing wave packet are associated with diffusive mixing across the transport barrier. At the lowest criticality, $\beta=0.24$, the PV gradients at the jet core are weaker, and spiral PV structures are apparent in Rossby wave critical layers to the jet flanks. No vortex shedding occurs across the jet at any point during the life cycle, the flow at the center of the channel remains laminar, and there is no transport across the material (PV) contour which has mean position $y=0$. It is important to emphasize that, nevertheless, the upper layer flow in the $\beta=0.24$ simulation, and indeed in all of the simulated flows up to and including $\beta=0.30$, becomes fully turbulent in the regions to the jet flanks with an associated vigorous mixing of PV.

The sensitivity of the upper layer barrier behavior to changes in β, seen in Fig. 4, is broadly consistent with calculated changes in the structure of the fastest growing linear normal mode of the initial state (see E08 for details of the normal mode calculations). As β is decreased, first the phase speed of the fastest growing normal mode increases,[37] bringing the upper layer critical lines closer to the jet core. Second, the upper layer wave amplitude, measured in terms of fluid particle displacements, increases relative to the wave amplitude in the lower layer. Both of these effects are consistent with increased mixing near the jet core in the upper layer during the baroclinic life cycle, and thus with the eventual breakdown of the mixing barrier as observed in Fig. 4. However, linear analysis of the initial state does not lead to (obvious) quantitative predictions for the value of β at which the barrier breakdown occurs.

In order that an objective comparison of transport barrier behavior can be made with the theoretical predictions outlined above, a normalized measure $\mathcal{R}$ can be defined as follows:

$$\mathcal{R} = 1 - \frac{\int_{q_1>0} q_1(x,y,T)d^2\mathbf{x}}{L_x \int_0^{L_y/2} Q_1(y)dy}, \tag{16}$$

where $T=300f_0^{-1}$ is the time taken as the end of the simulations, and the integration in the numerator is taken over that part of the channel where $q_1(x,y,T)>0$. The measure $\mathcal{R}$ is therefore constructed from the ratio of the positive PV, spatially integrated over the upper layer, at the end of the simulation to that at the beginning. If there is no mixing of PV whatsoever across the central mixing barrier, then the two integrals will be equal, yielding $\mathcal{R}=0$. If, on the other hand, complete homogenization of PV across the channel is attained, $q_1(x,y,T)$ will be zero everywhere, yielding $\mathcal{R}=1$. In the simulations, evaluation of $\mathcal{R}$ at earlier times ($t<T$), reveals that it increases rapidly during the "wave breaking" period of each life cycle (typically $80f_0^{-1}<t<220f_0^{-1}$) after which time it asymptotes to a near constant value toward the end of each life cycle.

Below, we compare theoretical predictions for the jet profiles $[\bar{u}_1(y)$ and $\bar{u}_2(y)]$, the change in the potential energy ratio V/E, the integrated upper layer cross-jet PV exchange $\mathcal{R}$, and the maximum jet velocities max $\{\bar{u}_1(y)\}$, max $\{\bar{u}_2(y)\}$, with values calculated from the simulations.

B. Theory and simulations: Direct comparison

The relevance and accuracy of the extended EPVH theory can be assessed by direct comparison with the numerical simulations. The theory in the robust barrier regime has been previously assessed for the case of a narrower channel ($L_y=5\pi$ as opposed to $L_y=7\pi$) in E08. Here, the focus is on the transition between the leaky and robust flow regimes and on flows with higher criticalities (lower β) than those considered in E08 in order to examine the breakdown of the mixing barrier. The increased channel width is necessary in order to avoid sidewall effects becoming important for the higher criticality flows. For lower criticality (higher β) flows the exact location of the sidewalls is unimportant and the final simulated jets are found to be almost independent of the sidewall location.

Figure 5 shows zonal mean wind profiles in each layer $[\bar{u}_1(y)$ and $\bar{u}_2(y)]$ at the end of the life cycle simulations for the $\sigma=2$ jet case ($T=300f_0^{-1}$, solid curves). The results from the simulations can be compared directly to the theoretical predictions (curves with squares) and with the initial flow in each layer (dotted curves). A moderate value of the smoothness parameter $\delta=1$ is used, as this value results a reasonable fit to the simulated jet profiles. Higher values of δ generate weaker, broader jets and lower values stronger, sharper ones, consistent with an increased or reduced width for the PV jump at the center of the upper layer, respectively.

The theoretical predictions derived from the nonlinear Eqs. (14) are largely successful in predicting the basic magnitude and cross-channel structure of the simulated jets in each layer. As β is decreased, the jet in the lower layer becomes stronger and wider, while retaining a similar latitudinal structure. The upper layer jet, however, undergoes a qualitative transition as the mixing barrier breaks down for flows $\beta \lesssim 0.20$. At higher values of β the profile near the jet core is approximately parabolic in shape, reflecting the fact the mixing regions are well away from the jet core. For $\beta < 0.20$, however, the jet profile is noticeably more "triangular" in the jet core region and the jet itself is much broader, consistent with PV mixing occurring right up to the jet core. The jet in the $\beta=0.12$ simulation shows some evidence of spontaneous symmetry breaking, a feature which is more pronounced in the simulations with a wider initial jet ($\sigma=3$).

Figure 6 shows the ratio of APE (V) to total energy (E) at the end of the simulations (squares) as a function of β for two different jet widths ($\sigma=2,3$). The horizontal lines in each panel show the ratio V_0/E_0 for the initial state. The curves show the corresponding theoretical predictions, derived from the solutions of Eq. (14) as above, for $\bar{V}/\bar{E}$ $(=\bar{V}/E_0)$ for three different values of the smoothness parameter δ. The theory is mainly successful in predicting the amount of potential energy released during the life cycle flows, and the predictions are relatively insensitive to the value of δ. No obvious transition is apparent between the robust and leaky regimes in the predictions for $\bar{V}/\bar{E}$, despite

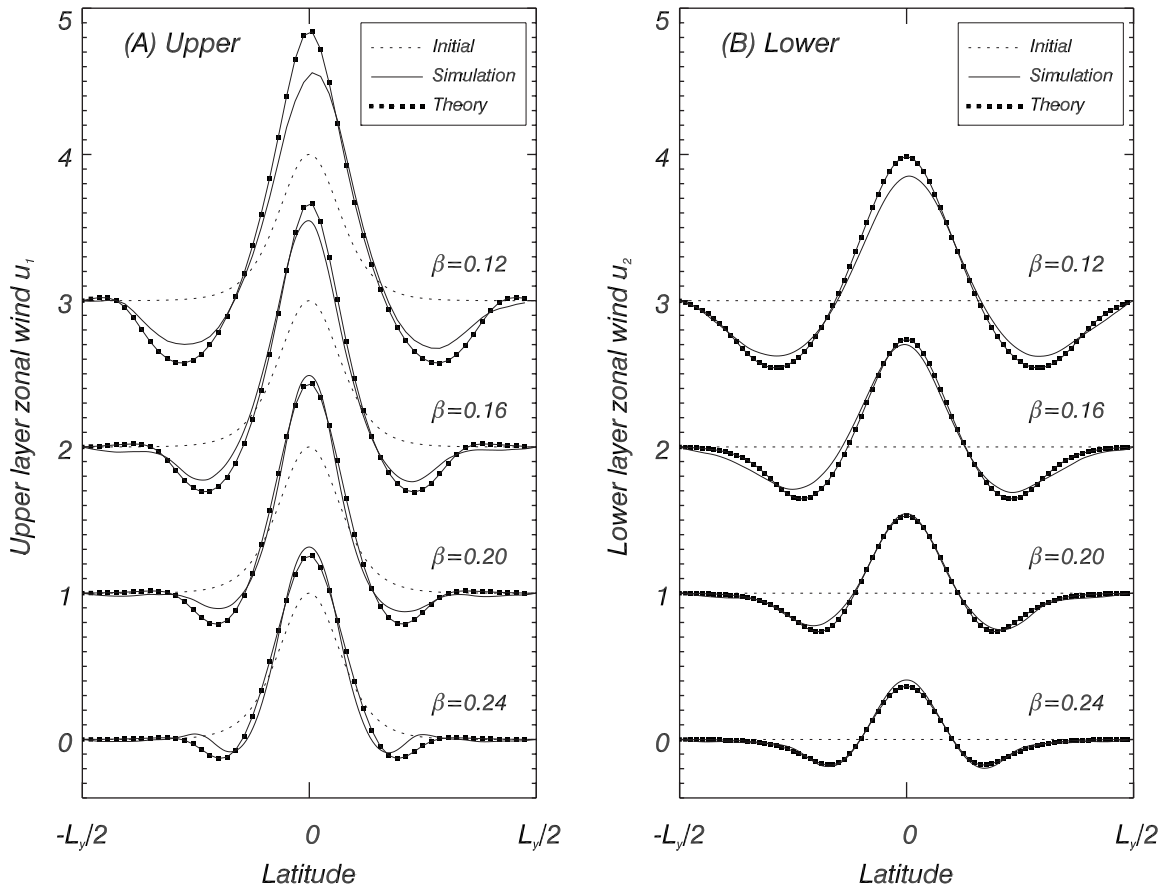

FIG. 5. Left: Zonal mean upper layer velocity $\bar{u}_1(y)$ at the end of the simulations ($t=300f_0^{-1}$, solid curves), the initial jet $U_1(y)$ (dotted curves), and the predictions from the theory with smoothness parameter $\delta=1$ (curves with squares). Right: Zonal mean lower layer velocity $[\bar{u}_2(y)]$ in the simulations and theory as above. In each panel, for clarity, the $\beta=0.12$, 0.16, and 0.20 results are offset by 3, 2, and 1 velocity units, respectively.

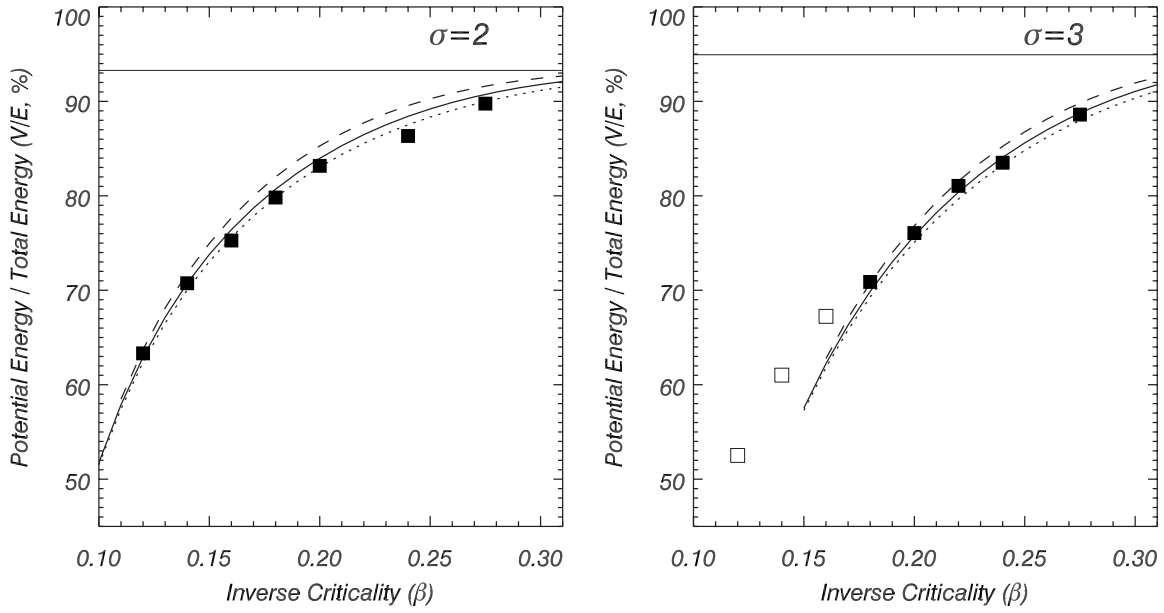

FIG. 6. The ratio of final potential energy V to final total energy E, expressed as a percentage, in the simulations (squares) and the corresponding theoretical predictions for $\bar{V}/\bar{E}$ derived from Eq. (14), plotted as a function of β for two different values of initial jet width $\sigma=2$ (left) and $\sigma=3$ (right). Theoretical predictions are for three different values of the smoothness parameter δ ($\delta=0.5$ dotted, $\delta=1$ solid, and $\delta=1.5$ dashed). The horizontal straight lines plotted in each panel correspond to the initial value of V/E at the beginning of the simulations. Unfilled squares correspond to simulations where there is significant symmetry breaking (see text).

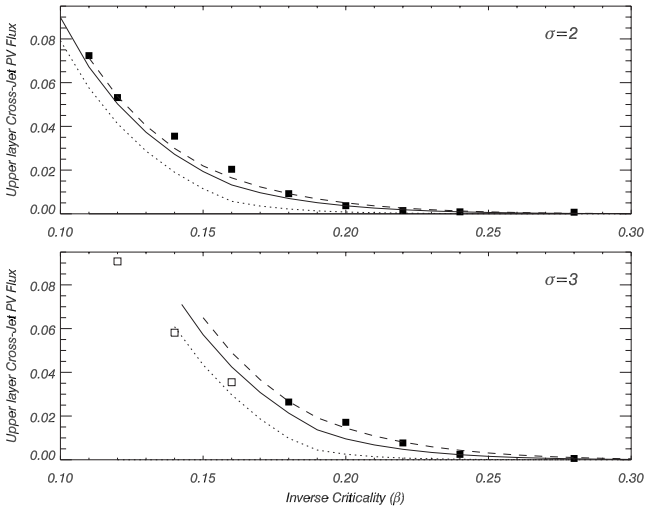

FIG. 7. Top: Integrated cross-jet PV exchange $\mathcal{R}$ as a function of β for the $\sigma=2$ simulations. Values calculated from the simulations (squares) and the theoretical predictions for different values of the smoothness parameter $\delta=0.5$, 1, and 1.5 (dotted, solid, and dashed) are plotted. Bottom: Same as in the top panel but for the $\sigma=3$ (wide jet) simulations. Unfilled squares correspond to simulations for which there is significant symmetry breaking (see text).

the mixing operator changing in character at $\beta\approx 0.16$ [see Eqs. (A2) and (A3)]. The theory is least successful in predicting the behavior of the wide jet ($\sigma=3$) at low β (unfilled squares). There appear to be two main reasons for the relatively poor agreement for these simulations. First, there is significant symmetry breaking in the final state [for example, selecting an objective measure, the integral quantity $\int|\bar{u}_1(y)-\bar{u}_1(-y)|dy$ is an order of magnitude higher for the low β, $\sigma=3$ final jets than for the other simulations]. Second, the return of energy to the zonal mean is somewhat inhibited and, consequently, for these flows it is difficult to say objectively that the life cycles have ended by $T=300f_0^{-1}$; note that Nakamura[37] investigated flows in which barotropic decay is inhibited or absent. One possible cause of the disagreement might be that sidewall effects are becoming important. For these flows the mixing regions extend nearly to the sidewalls and, in fact, the reason that the $\sigma=3$ theoretical predictions do not extend below $\beta\approx 0.14$ is that $Y_2, Y_3 \to L_y/2$. Another possible explanation for the relatively poor agreement with the theory is that it is due to a spontaneous breaking of latitudinal symmetry that is an observed feature of the very low β flows.

Figure 7 shows the integrated cross-jet upper layer PV exchange $\mathcal{R}$ (squares) as a function of β, calculated at the end of the simulations using Eq. (16), for jet widths $\sigma=2,3$. The corresponding theoretical predictions follow from the definition of the mixing operation (6) and the solution of Eq. (14), i.e.,

$$\mathcal{R}=1-\frac{\int_0^{L_y/2}\int_{-L_y/2}^{L_y/2}K_1(y,y'|\mathbf{Y},\delta)Q_1(y')dy'dy}{\int_0^{L_y/2}Q_1(y)dy}. \qquad (17)$$

For both jet widths the theory results in a relatively accurate prediction for $\mathcal{R}$, although the agreement is poorest for the $\sigma=3$, low β, "symmetry breaking" simulations described above (unfilled squares). For the remaining simulations, particularly at lower values of β, the agreement is closest for relatively high values of the smoothness parameter δ ($\gtrsim 1.5$). Direct comparison between the simulated and predicted final upper layer PV profile $\bar{q}_1(y)$ reveals that $\delta=1-1.5$ results in a reasonable fit to the simulated profiles, close to the value ($\delta=1$) that gave the best fit to the zonal mean wind profiles (see Fig. 5). It is to be emphasized that the transition in Fig. 7 between leaky barrier behavior ($\mathcal{R}>0$) and robust barrier behavior ($\mathcal{R}\approx 0$) does not correspond to a transition between turbulent and laminar flow throughout the upper layer. Even in those simulations with negligible $\mathcal{R}$, i.e., a near-perfect upper layer transport barrier, vigorous turbulence and PV mixing occurs at the jet flanks.

Figure 8 shows the maximum zonal wind at the end of the simulations, max $\{\bar{u}_1\}$ and max $\{\bar{u}_2\}$, as a function of β (squares) together with the corresponding theoretical predictions (curves). Compared to the potential energy ratio (V/E) and the integrated cross-jet PV exchange $\mathcal{R}$, the maximum zonal winds are relatively sensitive to details of the energetic cycle in the simulation and, consequently, the time T taken to mark the end of the life cycle, and also exhibit a weak sensitivity to the value of diffusivity parameter κ. At low β, therefore, it is somewhat more difficult to make a definitive comparison with the simulations. In Fig. 8 we have simply plotted the values of max $\{\bar{u}_1\}$ and max $\{\bar{u}_2\}$ at $T=300f_0^{-1}$. At low β the theory is relatively unsuccessful in predicting the maximum zonal winds in the upper layer. Somewhat better agreement might be obtained if a case-by-case examination of the energetic cycle of each simulation informed the choice of value of T, and better agreement might also result if a wider channel and a lower value of κ were used, both of which would require a higher numerical resolution simulation. However, it is doubtful whether much would be gained by such additional simulations, as the theoretical predictions of max $\{\bar{u}_1\}$ are also rather sensitive to the smoothness parameter δ. The impression that a better fit to the simulations is obtained at larger values of δ ($\gtrsim 1.5$) for lower β ($\lesssim 0.15$) and for smaller values of δ (≈ 0.5) for higher β is broadly supported by a detailed comparison of final PV profiles (not shown). Hence, despite the success of the theory in predicting jet profile shapes, potential energy release (V/E) and the integrated cross-jet PV exchange in the upper layer $(\mathcal{R})$, it is probably the case that additional heuristic detail is required if the theory is to make accurate predictions of the maximum zonal velocities at the end of the life cycles across a wide range of parameters.

V. CONCLUSIONS

The aim of this work has been to understand, through the development of a predictive theory, a highly nonlinear transition in the behavior of baroclinic life cycles. In a series of two-layer model simulations, it has been demonstrated that the horizontal barrier to transport and PV mixing at the upper layer jet core (the model tropopause) remains impermeable

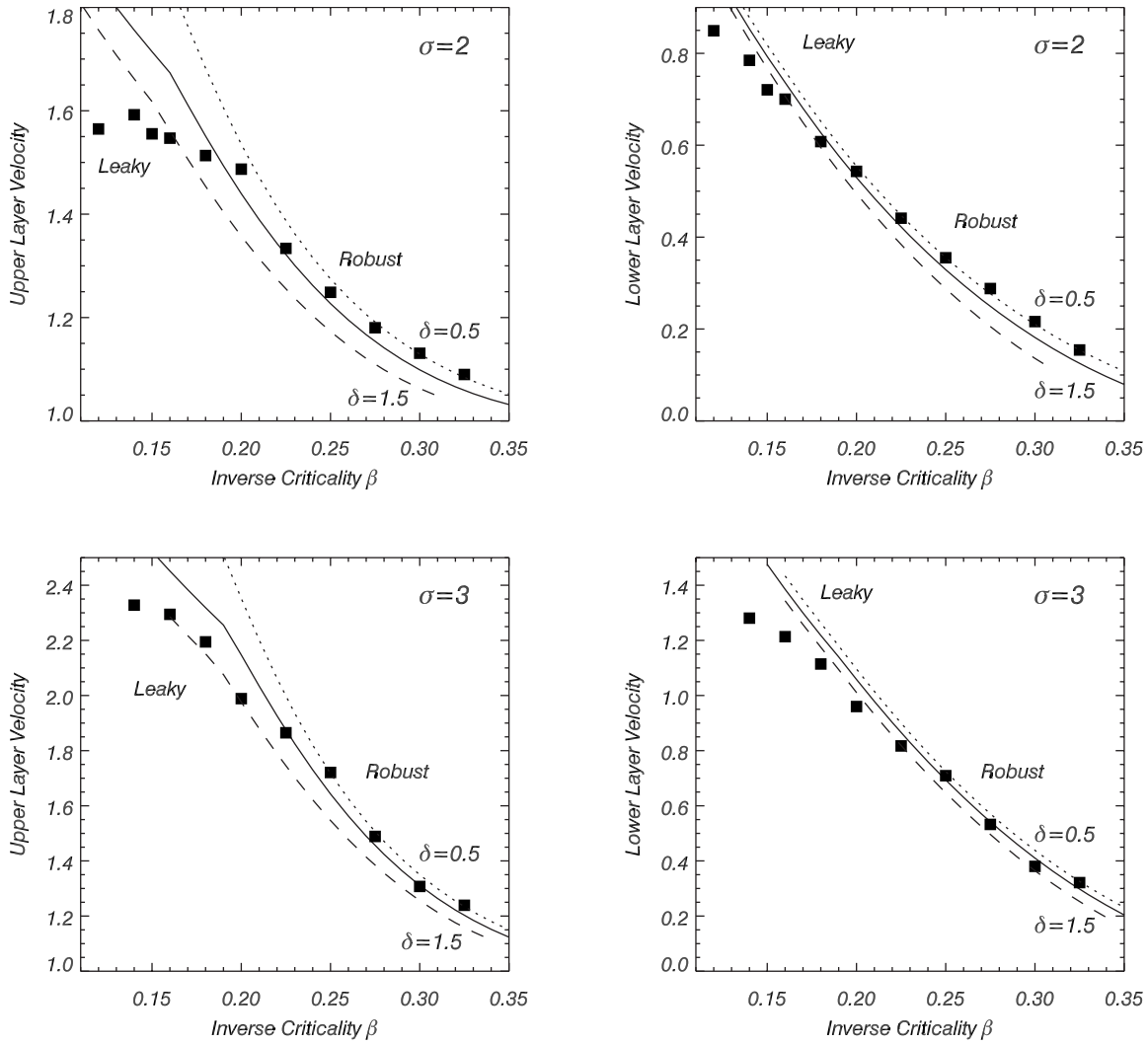

FIG. 8. (Upper panels) Left: Maximum upper layer jet strength max $\{\bar{u}_1\}$ as a function of the inverse criticality β for the $\sigma=2$ case. Predictions (curves) for different values of the smoothness parameter $\delta=0.5$, 1, and 1.5 (dotted, solid, and dashed) are plotted, along with the results of the simulations at $t=300f_0^{-1}$ (squares). Right: Theoretical and simulated lower layer jet strength max $\{\bar{u}_2(y)\}$, as in (a). (Lower panels) Same as in upper panels but for the $\sigma=3$ (wide jet) simulations.

to fluid transport, or robust, at low criticality (high β) but leaks at high criticality (low β). To investigate the transition in the barrier behavior a modified version of the EPVH theory of E08 (Ref. 25) has been used to make predictions for the equilibrated state at the end of the life cycles and, in particular, to predict the transition between the robust and leaky transport barrier regimes. The EPVH predictions are obtained by minimizing the APE of the flow, subject to constraints on the total momentum and energy, and the assumption that eddy-induced rearrangements of the initial PV field have the relatively simple effect of homogenizing the initial profile within well-delineated (but initially unspecified) regions.

The EPVH theory is found to successfully predict jet profiles and potential energy release as a function of the initial flow parameters. The theory also predicts the time-integrated PV transported across the jet core (see Fig. 7), providing new quantitative insight into the determination of the transport barrier properties. Knowledge of the cross-jet PV exchange might allow other physically important quantities such tracer fluxes across the jet to be estimated, for example, by using prior knowledge of the PV-tracer relationship. Most importantly, from a climate perspective, this work represents a step toward a quantitative understanding of the physical processes that control cross-jet transport in baroclinic flows in nature.

Despite the EPVH theory resulting in a relatively opaque set of equations (14), the guiding physical principle is relatively clear. Unstable baroclinic flows release APE by localized mixing of PV. This mixing proceeds until the source of APE contained in sloping isopycnal (or isentropic) surfaces, taking into account the global invariants of momentum and energy, is exhausted. It is clear, nonetheless, that the EPVH theory contains some heuristic elements that demand explanation. The occurrence of PV homogenization can be argued to be the only possible consequence of parcelwise PV conservation in a region of layerwise turbulent flow, and is a near-ubiquitous feature of high-resolution numerical simulations and analyzes of geophysical flows.[8,10,38] The fact that PV homogenization becomes localized to specific regions is

consistent with the Rossby wave elasticity argument of McIntyre[12] discussed above. That the mixing regions in the robust regime are organized as in Fig. 1(a) is consistent with a global, as opposed to a local, minimum of APE, subject to the constraints, being attained with this pattern. What is less clear is why, when the upper layer mixing regions in Fig. 1(a) come together in the leaky regime shown in Fig. 1(b), they coalesce to form a single region that is subdivided by a leaky transport barrier. In contrast, the "dynamically consistent," topographically forced, barotropic flows studied recently by Haynes *et al.*[24] are not characterized by leaky barrier behavior. Instead a robust barrier, present at low values of the controlling amplitude parameter, was abruptly destroyed at higher amplitudes. The reason for this qualitatively different behavior is unclear.

There is strong evidence that, as discussed in Sec. I, leaky horizontal barriers to transport exist in baroclinic flows in nature. It is naive to expect too close a correspondence between the idealized two-layer flows simulated here and those observed, but scale analysis reveals that energetic ocean currents, such as the North Atlantic Gulf Stream, have high criticality ($\beta \lesssim 0.05$). Consequently, based on the results above, it is perhaps unsurprising that repeated shedding of "warm-core" and "cold-core" vortices takes place across the current, as also seen in Fig. 4 (top panel). Note, however, using a similar idealized model formulation to the present one (a $2\frac{1}{2}$ layer model), Yuan *et al.*[19] demonstrated that with a different initial flow, robust upper layer barrier behavior can also occur for an unstable baroclinic flow at Gulf-stream parameter settings.

The transition between leaky and robust transport barriers, at somewhat lower criticalities ($0.15 \lesssim \beta \lesssim 0.25$), is arguably of more direct relevance to the extratropical tropopause barrier in the atmosphere. It is well documented[39] that mature extratropical cyclones can lead to wave breaking and mixing at the tropopause and that this can take one of two characteristic forms. Either thin filaments of stratospheric air are pinched off (in the so-called LC1 paradigm) or vortex roll-up similar to that seen in Fig. 4 can occur (the LC2 paradigm). LC1 is associated with significantly lower exchange of tropospheric and stratospheric air[40] and can be associated with the robust barrier regime, whereas LC2 is a clear example of leaky barrier behavior. Recent studies have revealed the observed LC1/LC2 ratio, and hence the barrier robustness, to correlate significantly with climate indices such as El Nino and the Southern Oscillation[41] and the North Atlantic Oscillation.[42] In addition, several different diagnostic methods have revealed the extratropical tropopause transport barrier to be substantially more robust during winter than summer.[15,20,21] Much remains to be done to understand this observed variability, including the extension of the present theory to more realistic forced-dissipative flows. Nevertheless, the current study suggests that such theoretical progress may well lead to predictive, quantitative theoretical descriptions of the mixing barrier behavior of observed atmospheric and oceanic flows.

ACKNOWLEDGMENTS

B. Willcocks and A. Thompson are acknowledged for helpful comments on this manuscript, and J. Vanneste for pointing out the original reference for the mixing operator.

APPENDIX: EXPLICIT EXPRESSIONS FOR THE MIXING KERNELS

The EPVH theory described above requires a specific form for the mixing operator $\mathcal{L}_i$ in Eq. (6). To define $\mathcal{L}_i$, the kernels of the Fredholm integral operator $K_i(y,y'|\mathbf{y},\delta)$ in Eq. (6) must be specified. A starting point in the construction of the kernels is to define a "smoothed top-hat" function

$$h(y|y_a,y_b,\delta) = \frac{1}{2}\left[\tanh\left(\frac{y-y_a}{\delta}\right) - \tanh\left(\frac{y-y_b}{\delta}\right)\right].$$

In the limit $\delta \to 0$, $h(y|y_a,y_b,0)$ is equal to unity for $y \in [y_a,y_b]$ and to zero outside this region. The effect of finite δ is to smooth the edges of the top hat. The integral of h across the channel can be written as

$$\begin{aligned}\bar{h}(y_a,y_b,\delta) &= \int_{-L_y/2}^{L_y/2} h(y|y_a,y_b,\delta)dy \\ &= \frac{\delta}{2}\log\left[\frac{\cosh[(L_y/2+y_b)/\delta]\cosh[(L_y/2-y_a)/\delta]}{\cosh[(L_y/2-y_b)/\delta]\cosh[(L_y/2+y_a)/\delta]}\right].\end{aligned}$$

A normalized, two-dimensional, smoothed top-hat function can then be defined as

$$H(y,y'|y_a,y_b,\delta) = \frac{h(y|y_a,y_b,\delta)h(y'|y_a,y_b,\delta)}{\bar{h}(y_a,y_b,\delta)}.$$

The functions above can be used to construct the kernels. For the lower layer ($i=2$) a suitable expression is

$$\begin{aligned}K_2(y,y'|y_3,\delta) &= H(y,y'|-y_3,y_3,\delta) \\ &\quad + [1-h(y|-y_3,y_3,\delta)]\delta_*(y-y'). \qquad \text{(A1)}\end{aligned}$$

Application of $\mathcal{L}_2[\mathbf{y},\delta]\cdot Q_2$ with the kernel (A1) results in a mixed profile with near-homogeneous PV between latitudes $-y_3$ and y_3.

For the upper layer, it is necessary to define a kernel K_1 that takes a different form in the robust and leaky regimes. The value of y_1, which in the robust regime defines the inner boundary of the upper layer mixing regions [see Fig. 1(a)], can be used to differentiate between the two regimes. For the robust regime ($y_1 > \delta$), we take

$$\begin{aligned}K_1(y,y'|y_1,y_2,\delta) &= H(y,y'|y_1,y_2,\delta) + H(y,y'|-y_2,-y_1,\delta) \\ &\quad + [1-h(y|-y_2,-y_1,\delta) \\ &\quad - h(y|y_1,y_2,\delta)]\delta_*(y-y') \\ &\quad (y_1 > \delta, \text{ robust regime}), \qquad \text{(A2)}\end{aligned}$$

where $\delta_*(y)$ is the Dirac delta function, whereas for the leaky regime ($y_1 \leq \delta$),

$$K_1(y,y'|y_1,y_2,\delta) = (1-\alpha)[H(y,y'|\delta,y_2,\delta) + H(y,y'|-y_2,-\delta,\delta)] + \alpha H(y,y'|-y_2,y_2,\delta)$$
$$+ \{1-(1-\alpha)[h(y|-y_2,-\delta,\delta) + h(y|\delta,y_2,\delta)] - \alpha h(y|-y_2,y_2,\delta)\}\delta_*(y-y') \quad (y_1 \le \delta, \text{ leaky regime}). \tag{A3}$$

Here, $\alpha(y_1,y_2,\delta)=(\delta-y_1)/(y_2+\delta)$ is a measure, with $0\le\alpha\le 1$, that controls the extent of the leakage across the barrier. The action of the mixing operator defined by Eqs. (A2) and (3) on a particular initial profile is illustrated in Fig. 2 (see main text).

Note that both K_1 and K_2 are non-negative everywhere and their integrals across the channel in y and y' are unity. Hence, they are suitable kernels for a mixing operator. It is also straightforward to obtain their derivatives with respect to the latitude parameters y_1, y_2, etc., for use in Eq. (15). For example,

$$\frac{\partial K_2}{\partial y_3}(y,y'|y_3,\delta) = \frac{h(y|-y_3,y_3,\delta)h'(y'|-y_3,y_3,\delta) + h'(y|-y_3,y_3,\delta)h(y'|-y_3,y_3,\delta)}{\bar{h}(-y_3,y_3,\delta)}$$
$$- \frac{-\bar{h}'(-y_3,y_3,\delta)h(y|-y_3,y_3,\delta)h(y'|-y_3,y_3,\delta)}{\bar{h}(-y_3,y_3,\delta)^2} - h'(y|-y_3,y_3,\delta))\delta_*(y-y'),$$

where

$$h'(y|y_a,y_b,\delta) = \frac{\partial h}{\partial y_b}(y|y_a,y_b,\delta) - \frac{\partial h}{\partial y_a}(y|y_a,y_b,\delta).$$

Similar explicit results for $\partial K_1/\partial y_1$ and $\partial K_1/\partial y_2$ complete the set needed to evaluate Eq. (15).

[1] P. B. Rhines, "Waves and turbulence on the beta plane," J. Fluid Mech. **69**, 417 (1975).
[2] P. B. Rhines, "Jets," Chaos **4**, 313 (1994).
[3] N. A. Maximenko, B. Bang, and H. Sasaki, "Observational evidence of alternative zonal jets in the world ocean," Geophys. Res. Lett. **32**, L12607, DOI: 10.1029/2005GL022728 (2005).
[4] K. J. Richards, N. A. Maximenko, F. O. Bryan, and H. Sasaki, "Zonal jets in the pacific ocean," Geophys. Res. Lett. **33**, L03605, DOI: 10.1029/2005GL024645 (2006).
[5] J. Marshall, E. F. Shuckburgh, H. E. Jones, and C. Hill, "Estimates and implications of surface eddy diffusivity in the southern ocean derived from tracer transport," J. Phys. Oceanogr. **36**, 1806 (2006).
[6] P. S. Marcus, "Jupiter's great red spot and other vortices," Annu. Rev. Astron. Astrophys. **31**, 523 (1993).
[7] G. P. Williams, "Jovian dynamics. Part III: Multiple, migrating, and equatorial jets," J. Atmos. Sci. **60**, 1270 (2003).
[8] R. K. Scott and L. M. Polvani, "Forced-dissipative shallow-water turbulence on the sphere and the atmospheric circulation of the giant planets," J. Atmos. Sci. **64**, 3158 (2007).
[9] T. Dunkerton and R. K. Scott, "A barotropic model of the angular momentum conserving potential vorticity staircase in spherical geometry," J. Atmos. Sci. **65**, 1105 (2008).
[10] D. G. Dritschel and M. E. McIntyre, "Multiple jets as PV staircases: The Phillips effect and the resilience of eddy-transport barriers," J. Atmos. Sci. **65**, 855 (2008).
[11] K. S. Smith, "Tracer transport along and across coherent jets in two-dimensional turbulent flow," J. Fluid Mech. **544**, 133 (2005).
[12] M. E. McIntyre, "The quasi-biennial oscillation (QBO): Some points about the terrestrial QBO and the possibility of related phenomena in the solar interior," in *The Solar Engine and Its Influence on the Terrestrial Atmosphere and Climate*, NATO Advanced Studies Institute, Series I: Global Environmental Change (Springer-Verlag, Berlin, 1994), Vol. 25, Chap. 2, pp. 293–320.
[13] R. K. Scott and J.-P. Cammas, "Wave breaking and mixing at the subtropical tropopause," J. Atmos. Sci. **59**, 2347 (2002).
[14] N. Nakamura, "Two-dimensional mixing, edge formation, and permeability diagnosed in area coordinates," J. Atmos. Sci. **53**, 1524 (1996).
[15] P. H. Haynes and E. F. Shuckburgh, "Effective diffusivity as a diagnostic of atmospheric transport. Part II: Troposphere and lower stratosphere," J. Geophys. Res. **105**, 22795, DOI: 10.1029/2000JD900092 (2000).
[16] P. H. Haynes and E. F. Shuckburgh, "Effective diffusivity as a diagnostic of atmospheric transport. Part I: Stratosphere," J. Geophys. Res. **105**, 22777, DOI: 10.1029/2000JD900093 (2000).
[17] A. S. Bower, H. T. Rossby, and J. L. Lillibridge, "The Gulf Stream: Barrier or blender?" J. Phys. Oceanogr. **15**, 24 (1985).
[18] A. S. Bower and M. S. Lozier, "A closer look at particle exchange in the Gulf Stream," J. Phys. Oceanogr. **24**, 1399 (1994).
[19] G.-C. Yuan, L. J. Pratt, and C. K. R. T. Jones, "Cross-jet Lagrangian transport and mixing in a 2 1/2 -layer model," J. Phys. Oceanogr. **34**, 1991 (2004).
[20] G. Berthet, J. G. Esler, and P. H. Haynes, "A Lagrangian perspective of the tropopause and the ventilation of the lowermost stratosphere," J. Geophys. Res. **112**, D18102, DOI: 10.1029/2006JD008295 (2007).
[21] P. Chen, "Isentropic cross-tropopause mass exchange in the extratropics," J. Geophys. Res. **100**, 16661, DOI: 10.1029/95JD01264 (1995).
[22] M. D. Greenslade and P. H. Haynes, "Vertical transition in transport and mixing in baroclinic flows," J. Atmos. Sci. **65**, 1137 (2008).
[23] R. T. Pierrehumbert, "Chaotic mixing of tracer and vorticity by modulated travelling Rossby waves," Geophys. Astrophys. Fluid Dyn. **58**, 285 (1991).
[24] P. H. Haynes, D. Poet, and E. F. Shuckburgh, "Transport and mixing in dynamically consistent flows," J. Atmos. Sci. **64**, 3640 (2007).
[25] J. G. Esler, "The turbulent equilibration of an unstable baroclinic jet," J. Fluid Mech. **599**, 264 (2008).
[26] N. A. Phillips, "A simple three-dimensional model for the study of large-scale extratropical flow patterns," J. Meteorol. **8**, 381 (1951).
[27] J. Pedlosky, *Geophysical Fluid Dynamics* (Springer-Verlag, New York, 1987).
[28] S. Lee and I. M. Held, "Baroclinic wave packets in models and observations," J. Atmos. Sci. **50**, 1413 (1993).
[29] V. Pavan and I. M. Held, "The diffusive approximation for eddy fluxes in baroclinically unstable jets," J. Atmos. Sci. **53**, 1262 (1996).
[30] I. M. Held, "Progress and problems in large-scale atmospheric dynamics," *The Global Circulation of the Atmosphere: Phenomena, Theory, Challenges* (Princeton University Press, Princeton, 2007), Chap. 1.
[31] J. G. Esler and P. H. Haynes, "Mechanisms for wave packet formation and maintenance in a quasi-geostrophic two-layer model," J. Atmos. Sci. **56**, 2457 (1999).
[32] N. Nakamura, "Baroclinic-barotropic adjustments in a meridionally wide domain," J. Atmos. Sci. **56**, 2246 (1999).
[33] V. I. Arnold and B. A. Khesin, *Topological Methods in Hydrodynamics*, Applied Mathematical Series (Springer-Verlag, New York, 1998).
[34] A. I. Shnirelman, "Lattice theory and flows of ideal incompressible fluids," Russ. J. Math. Phys. **1**, 105 (1993).

[35]W. H. Press, S. A. Teukolsky, W. T. Vetterling, and B. P. Flannery, *Numerical Recipes in Fortran 77*, 2nd ed. (Cambridge University Press, Cambridge, 1996).
[36]A. J. Simmons and B. J. Hoskins, "The lifecycles of some nonlinear baroclinic waves," J. Atmos. Sci. **35**, 414 (1978).
[37]N. Nakamura, "Momentum flux, flow symmetry, and the nonlinear barotropic governor," J. Atmos. Sci. **50**, 2159 (1993).
[38]P. B. Rhines and W. R. Young, "Homogenization of potential vorticity in planetary gyres," J. Fluid Mech. **122**, 347 (1982).
[39]C. D. Thorncroft, B. J. Hoskins, and M. E. McIntyre, "Two paradigms of baroclinic wave life-cycle behaviour," Q. J. R. Meteorol. Soc. **119**, 17 (1993).
[40]L. M. Polvani and J. G. Esler, "Transport and mixing of chemical airmasses during idealized baroclinic lifecycles," J. Geophys. Res. **112**, D23102, DOI: 10.1029/2007JD008555 (2007).
[41]M. Shapiro, H. Wernli, N. Bond, and R. Langland, "The influence of the 1997–1998 ENSO on extratropical baroclinic life cycles over the Eastern North Pacific," Q. J. R. Meteorol. Soc. **127**, 331 (2001).
[42]C. Franzke, S. Lee, and S. B. Feldstein, "Is the North Atlantic oscillation a breaking wave?" J. Atmos. Sci. **61**, 145 (2004).